

# 4 ANALYSIS AND MODELING

## 4.1 TRANSIENT ABSORPTION AND ANISOTROPY

Short laser pulses, used in pump-probe experiments, generally consist of a range of frequencies that are selectively absorbed as they travel through the sample. In pump-probe spectroscopy we measure the frequency-resolved transmission spectra of probe pulses through the sample. To compensate for pulse to pulse fluctuations of the laser system the probe is split before the sample into probe and reference pulses. The reference pulses are sent through the sample before the pump pulses. The probe is spatially overlapped with the pump and focussed in the sample. The relative delay time between pump and probe pulses is controlled with a delay stage. To determine the pump-induced changes of the probe transmission, the signals are alternatingly measured with and without the pump pulse present using a chopper in the pump beam before the sample. The pump-induced relative transmissions are calculated from two subsequent probe measurements using

$$\frac{T(t, \nu)}{T_0(\nu)} = \frac{I_{\text{probe}}(t, \nu)/I_{\text{ref}}(\nu)}{I_{0,\text{probe}}(\nu)/I_{0,\text{ref}}(\nu)}, \quad (4.1)$$

where  $I_{\text{probe}}$  and  $I_{\text{ref}}$  are the probe and reference intensities measured by the detector and the subscript 0 indicates that the pump was blocked for those probe shots. From these relative transmissions we calculate the pump-induced absorption changes using Lambert-Beer law (Eq. (2.22)):

$$\Delta\alpha(t, \nu) = -\ln(T(t, \nu)/T_0(\nu)). \quad (4.2)$$

We have seen in Eq. (2.49) that the absorption cross-section of infrared active modes, such as the O–H stretch vibration, is dependent on the directional overlap ( $\cos^2(\theta)$ ) between the transition dipole moment of the absorbing oscillator and the polarization of the light. A linearly polarized pump beam thus excites an anisotropic distribution of transitions in an isotropic sample. We probe the anisotropic absorption differences ( $\Delta\alpha$ ) caused by this distribution using a pair of probe beams with parallel ( $\parallel$ ) and perpendicular ( $\perp$ ) polarizations with respect to the pump. In our experiments this is achieved by rotating the polarization of the pump with a  $\lambda/2$ -plate to  $45^\circ$  with respect to the probe polarization and selecting parallel and perpendicular probe components with a polarizer after the sample.

It can be shown [85] that if we take the following linear combinations of these absorptions we can retrieve separately the isotropic signal  $\Delta\alpha$  and the

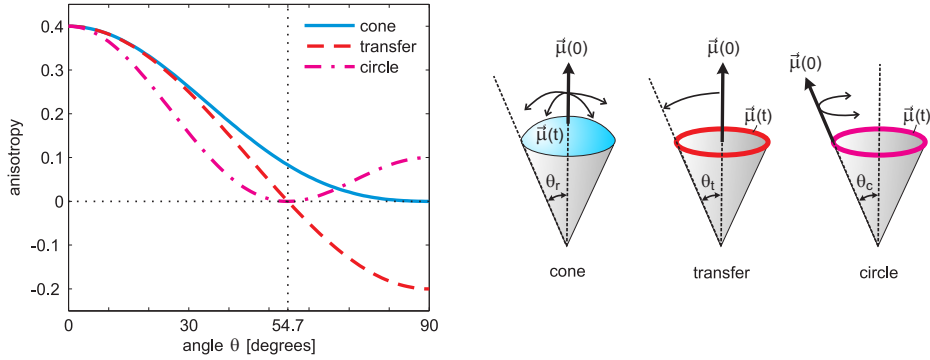


FIGURE 4.1. Dependence of the anisotropy on the reorientation angle  $\theta$  of the transition dipole moment  $\vec{\mu}$ . The initial and final directions are indicated by  $\vec{\mu}(0)$  and  $\vec{\mu}(t)$ , respectively.

anisotropy  $R$ :

$$\Delta\alpha(t, \nu) = \frac{\Delta\alpha_{\parallel}(t, \nu) + 2 \cdot \Delta\alpha_{\perp}(t, \nu)}{3}, \quad (4.3)$$

$$R(t, \nu) = \frac{\Delta\alpha_{\parallel}(t, \nu) - \Delta\alpha_{\perp}(t, \nu)}{\Delta\alpha_{\parallel}(t, \nu) + 2 \cdot \Delta\alpha_{\perp}(t, \nu)}. \quad (4.4)$$

The isotropic signal depends only on the density of the pump-induced absorption differences and is independent of rotational diffusion. Conversely, the anisotropy is proportional to the second-order orientational correlation function of the direction of the excitation and equals [85]:

$$R(t) = \frac{2}{5} \langle P_2(\hat{\mu}(0) \cdot \hat{\mu}(t)) \rangle \quad (4.5)$$

where  $\hat{\mu}(0) \cdot \hat{\mu}(t)$  is the inner product between unit vectors along the direction of transition dipole moments at times 0 and  $t$ .  $P_2(x) = \frac{1}{2} (3x^2 - 1)$  is the second Legendre polynomial and  $\langle \dots \rangle$  denotes the ensemble average. From the isotropic signal we obtain information about the vibrational relaxation rate  $k$  which depends on the density and cross-section of nearby accepting modes. The anisotropic signal reveals information about reorientational motion (or lack thereof) as well as vibrational Förster energy transfer.

From Eqs. (4.3) and (4.4) it can be shown that when the pump-probe signal consists of multiple components that have different anisotropies, the total observed anisotropy will be the average of the individual anisotropies  $R_i$ , weighted with the isotropic intensities  $\Delta\alpha_i$ :

$$R_{\text{total}} = \frac{\sum_i \Delta\alpha_i \cdot R_i}{\sum_i \Delta\alpha_i} \quad (4.6)$$

In polarization resolved pump-probe spectroscopy, the observed anisotropy  $R$  depends on the average angular displacement of the transition dipole moment

as a result of reorientation or energy transfer. Using Eq. (4.5), we calculate this dependence for some of the most common scenarios, shown in Fig. 4.1:

$$R_{\text{cone}} = \frac{2}{5} \left( \frac{1}{2} \cos(\theta_r) \cdot [1 + \cos(\theta_r)] \right)^2, \quad (4.7)$$

$$R_{\text{transfer}} = \frac{1}{5} \left( 3 \cos^2(\theta_t) - 1 \right), \quad (4.8)$$

$$R_{\text{circle}} = \frac{1}{10} \left( 3 \cos^2(\theta_c) - 1 \right)^2. \quad (4.9)$$

From Eq. (4.7) it follows that when the excitation is uniformly distributed over all angles ( $\theta_c = 90^\circ$ ) the anisotropy is zero, i.e. isotropic. From Eq. (4.8) and Fig. 4.1, we note that when the excitation is at the 'magic angle' ( $\arccos(\sqrt{1/3}) = 54.7^\circ$ ) with respect to the pump polarization, the observed anisotropy will be zero. This is true both if the polarization jumped as a result of energy transfer, or if pump and probe were at this magic angle from the start. The observed anisotropy is then always zero and the probed absorption changes will be independent of reorientational diffusion. Note also that when the excitation jumps over an angle larger than  $54.7^\circ$ , the observed anisotropy can become negative, i.e.  $\Delta\alpha_{\parallel} < \Delta\alpha_{\perp}$ . From Fig. 4.1 we note that the anisotropy in Eq. (4.9) is not a bijective function of the angle  $\theta_r$  for  $R < 0.1$ , i.e. there are multiple angles corresponding to the same anisotropy. More specific distributions of  $\vec{\mu}$  can always be calculated using Eq. (4.5).

## 4.2 MULTI-COMPONENT ANALYSIS

In Section 4.1 we introduced the time and frequency dependent absorption difference spectra  $\Delta\alpha(t, \nu)$  measured in our pump-probe experiments. These transient spectra result from time-dependent spectral signatures reflecting non-equilibrium physical processes caused by the pump beam, such as the excitation of a vibrational mode. The shape of these spectral signatures may themselves also be time dependent, such as in the case of spectral diffusion or coherent artifacts. In most other cases we can treat these shapes as time-independent.

The amplitude and spectral shape of the transient spectrum reflects the frequency-dependent absorption cross-section of individual excited modes and the time-dependence of their excitations. In a macroscopic sample the time-dependence of individual excitations that have the same characteristics are averaged out and can be described as a single component. Such a component consist of a time-dependent population (i.e. concentration), proportional to the number of contributing excitations and a frequency dependent spectral signature, proportional to the absorption change resulting from this excitation. The response of each component  $i$  is thus the product of its population dynamics  $N_i(t)$  and spectral signatures  $\sigma_i(\nu)$ , while the total absorption change is the sum of these responses:

$$\Delta\alpha(t, \nu) = \sum_i N_i(t) \cdot \sigma_i(\nu). \quad (4.10)$$

This equation can be written in the form of a matrix equation as shown in Fig. 4.2

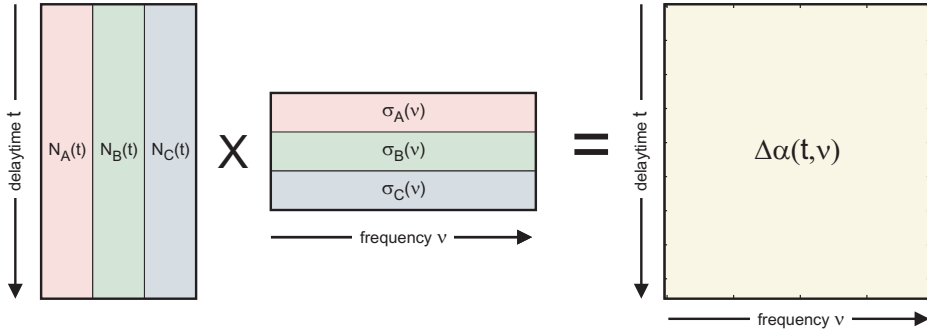


FIGURE 4.2. Decomposition of a three state model.

In general, a model that describes a data set is based on 'physical intuition', i.e. an understanding of the system under study and the general qualitative trends observed in the data. However, if a data set is congested with multiple overlapping spectral and temporal components we need a more rigorous set of tools to disentangle the observations. Thus, in order to analyze a multi-component data set, it is often necessary to isolate the dynamics and spectral signatures of its individual components.

#### 4.2.1 SINGULAR VALUE DECOMPOSITION

Before we can isolate the constituent components, we first need to estimate the number of components that are present in the data. A useful mathematical tool for this is called 'singular value decomposition' (SVD). It can be shown [106] that for any  $m \times n$  matrix  $M$  there exists a factorization of the form:

$$M = T S V \quad (4.11)$$

where  $T$  is an  $m \times m$  unitary matrix, the matrix  $S$  is a nonnegative  $m \times n$  diagonal matrix, and  $V$  is an  $n \times n$  unitary matrix. The columns of  $T$  and the rows of  $V$  can be viewed as orthonormal basis vectors with which to construct the constituent components in  $M$ . The weight of each component is given by the diagonal entries in matrix  $S$  which are called the singular values. To clarify this point we write Eq. (4.11) as:

$$M_{mn} = \sum_i T_{mi} \times S_{ii} \times V_{in}, \quad (4.12)$$

where the subscripts denote the coordinates of the matrix.

The singular values can be used to determine the total number of significant components in a data set. Substituting the data matrix  $\Delta\alpha(t, \nu)$  for  $M$  in Eq. (4.12), results in a decomposition of the data into orthonormal time-dynamics and spectral components, as column vectors in  $T$  and row vectors in

$V$ , respectively. It should be clear, however, that these vectors are in general not the 'real', temporal and spectral components that we wish to find, rather they are an orthonormal basis of said components. Nevertheless the singular values indicate how many components are needed to describe in principle a data set with any degree of accuracy.

The fractional contribution of each component is obtained by normalizing the vector of singular values:

$$\hat{S}_i = S_{ii}/(\sum_i S_{ii}). \quad (4.13)$$

In a completely noise-free data set the number of non-zero singular values directly reflect the number of constituent components. However, in a real data set it may not always be possible to unambiguously distinguish the lowest amplitude signal components from the noise (background) components. As a rule of thumb we look for those components that are significantly higher than the rest. As a simple example, we suppose a noisy data set that consists of the following (normalized) singular values:

$$\hat{S}_i = [0.78, 0.14, 0.05, 0.013, 0.011, 0.006].$$

Inspection of the first three singular values reveals that  $0.78+0.14+0.05 = 97\%$  of the signals in this data set can be described as a sum of three components. The third component is still significantly above the rest ( $0.05 > 3 \times 0.013$ ), while any additional components can not be sufficiently distinguished from the noise background.

#### 4.2.2 LEAST-SQUARES FITTING

After having established the number of components in the system, we remain with the task of finding a suitable model for the decomposition of our data set. There are several strategies that can be used. In general, we measure a data set  $\Delta\alpha(t, \nu)$  with standard deviations  $\epsilon(t, \nu)$  and wish to decompose and fit it using a multi component model. Each component  $i$  consist of a product of time dynamics  $N_i(t)$  and spectral shapes  $\sigma_i(\nu)$ , which depending on the model can depend on a set of parameters  $\mathbf{p}$ . To estimate how well a given model is fitted to a data set we use the chi-squared ( $\chi^2$ ) function, defined as the squared average number of standard deviations between data and model:

$$\chi^2(\mathbf{p}) = \int \int dt d\nu \left( \frac{\Delta\alpha(t, \nu) - \sum_i N_i(t; \mathbf{p}) \sigma_i(\nu; \mathbf{p})}{\epsilon(t, \nu)} \right)^2 \quad (4.14)$$

Because the time-dynamics and spectral shapes are dependant on the model parameters, so is the  $\chi^2$  function. Obviously, the best estimation for the values of these model parameters are those that minimize the  $\chi^2$  function. Following the definition of standard deviation, the minimum value that a  $\chi^2$  can reach for a perfect model is 1. In practice these values are higher because a model is usually a simplified description of reality. If the value is lower than 1, this indicates that either the standard deviations were overestimated or the model contained

too many parameters. There are several methods to find the minimum of a  $\chi^2$  function that can be broken down into numerical and analytical categories.

Concerning numerical methods, there exist computer algorithms that iteratively try to minimize the  $\chi^2$  by varying the parameter values. Such algorithms work analogous to a ball on an  $N$ -dimensional landscape (where  $N$  is the number of parameters) trying to find the lowest point by rolling down the hill. Just like a ball can get stuck in a hole, so the algorithm can get trapped in a local minimum. This is especially true if the model is complicated with many parameters or if the parameters display a large degree of covariance, i. e. changing one parameter value affects the  $\chi^2$  minimum as a function of another parameter. To remedy this, it is necessary to provide the fit algorithm with a suitable set of initial values and boundary conditions.

In the following we describe a number of analytical least-squares decomposition methods with which we directly calculate the best fitting model (spectra, time-dynamics, anisotropy) to a given set of data. The obvious advantage is that these methods do not require an iterative procedure and that they provide a unique solution (independent of starting values). Obviously it is not possible to unambiguously distinguish (deconvolve) two processes that behave in exactly the same way. Therefore least-squares decomposition is only possible if either the population dynamics or spectral signatures are linearly independent from one component to the other. In other cases, we need to impose or constrain either the spectral signatures or time dynamics.

### 4.2.3 SPECTRAL DECOMPOSITION

We start with the spectral decomposition, i. e. a set of spectra  $\sigma_i(\nu)$  that best fit a given set of population dynamics  $N_i(t)$  to data points  $\Delta\alpha(t, \nu)$  with standard deviations  $\epsilon(t, \nu)$ . To this end we define a function  $\chi^2$  that we need to minimize:

$$\chi^2(\tilde{\sigma}_i) = \int dt \left( \frac{\Delta\alpha(t, \nu) - \sum_i N_i(t) \cdot \tilde{\sigma}_i}{\epsilon(t, \nu)} \right)^2 \quad (4.15)$$

where  $\tilde{\sigma}_i$  are now  $i$  separate variables that are proportional to the relative spectral amplitudes at frequency  $\nu$ . The least squares fitting linear combination can be calculated by equating the derivatives with respect to these amplitudes to zero:

$$\frac{d}{d\tilde{\sigma}_i} \int dt \left( \frac{\Delta\alpha(t, \nu) - \sum_i N_i(t) \cdot \tilde{\sigma}_i}{\epsilon(t, \nu)} \right)^2 = 0 \quad (4.16)$$

This gives us  $i$  equations with  $i$  unknowns that may be readily solved. Repeating this procedure for all frequencies results in  $i$  separate spectral signatures  $\tilde{\sigma}_i(\nu)$ . An example of this procedure is shown in Fig. 4.3.

### 4.2.4 TEMPORAL DECOMPOSITION

Equivalently, this procedure will also work the other way around. If we know (or fit) the spectral signatures  $\sigma_i(\nu)$ , we can calculate the unknown population

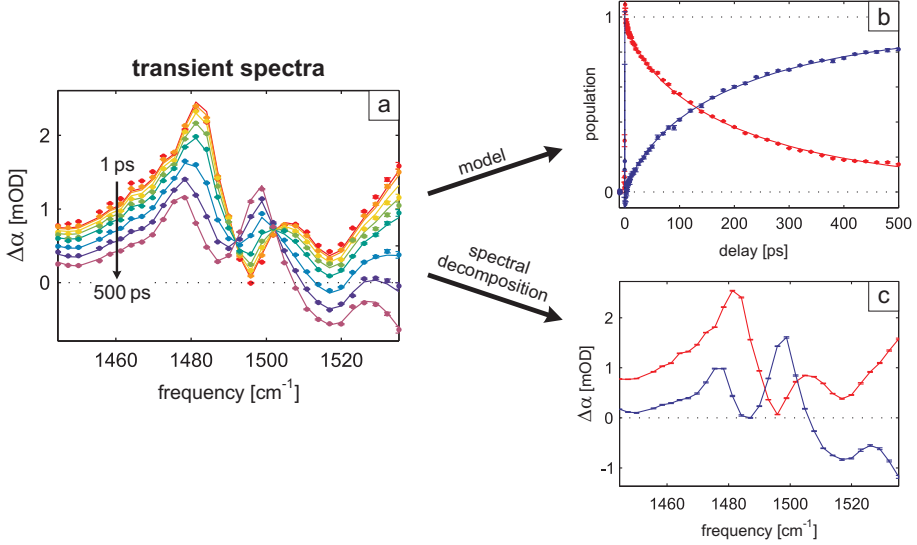


FIGURE 4.3. Decomposition of arbitrary data set into population dynamics and spectra. The population dynamics  $N(t)$  were modeled (lines **b**) and the least squares corresponding spectra  $\sigma(\nu)$  were extracted using spectral decomposition (**c**). The difference between the model  $N(t) \times \sigma(\nu)$  and data (lines and points **a**, respectively) were minimized. As a final check we reverse the process by calculating the temporal decomposition that correspond to the extracted spectra (points **b**).

dynamics  $\tilde{N}_i(t)$ :

$$\frac{d}{d\tilde{N}_i} \int d\nu \left( \frac{\Delta\alpha(t, \nu) - \sum_i \tilde{N}_i \cdot \sigma_i(\nu)}{\epsilon(t, \nu)} \right)^2 = 0 \quad (4.17)$$

This will yield  $i$  time traces  $\tilde{N}_i(t)$  that describe how a given set of spectra  $\sigma_i(\nu)$  are individually evolving in data set  $\Delta\alpha(t, \nu)$ , without the need for any kinetic modeling or knowledge of initial conditions.

#### 4.2.5 ANISOTROPIC DECOMPOSITION

Let us now assume two data sets  $\Delta\alpha_{\parallel}(t, \nu)$  and  $\Delta\alpha_{\perp}(t, \nu)$  that differ only in the amplitude of their spectral response as a result of a component-specific time-dependent (frequency-independent) anisotropy  $R_i(t)$ :

$$\Delta\alpha_{\parallel}(t, \nu) = \sum_i (1 + 2R_i(t)) N_i(t) \cdot \sigma_i(\nu) \equiv \sum_i N_{i,\parallel}(t) \cdot \sigma_i(\nu) \quad (4.18)$$

$$\Delta\alpha_{\perp}(t, \nu) = \sum_i (1 - R_i(t)) N_i(t) \cdot \sigma_i(\nu) \equiv \sum_i N_{i,\perp}(t) \cdot \sigma_i(\nu) \quad (4.19)$$

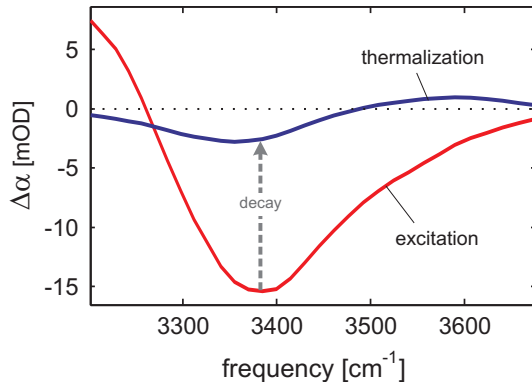


FIGURE 4.4. . Two spectral signatures typically found in pump-probe experiments on water. The excitation of the O–H stretch vibration leads to direct absorption changes associated with the transition  $\nu = 0 \rightarrow 1$ . The subsequent thermalization leads to indirect absorption changes resulting from the anharmonic coupling of low frequency modes to the ground state  $\nu = 0$  of the O–H stretch mode.

It can be easily shown that the isotropic signal defined by Eq. (4.3) is independent of  $R_i(t)$ . It can be also shown, using Eq. (4.4), that if the anisotropy dynamics are the same for all components (i.e.  $R_i(t) = R(t)$ ), we retrieve a frequency independent anisotropy.

In any case, if we know the spectra  $\sigma_i(\nu)$ , e.g. through spectral decomposition of the *isotropic* data, we can use temporal decomposition on both  $\parallel$  and  $\perp$  data sets to calculate the values of  $N_{i,\parallel}(t)$  and  $N_{i,\perp}(t)$  for all  $i$  and  $t$ . Having retrieved these anisotropic populations, we can use the following familiar linear combination (cf. Eq. (4.4)) to isolate the component-specific anisotropy  $R_i(t)$ :

$$R_i(t) = \frac{N_{i,\parallel}(t) - N_{i,\perp}(t)}{N_{i,\parallel}(t) + 2N_{i,\perp}(t)} \quad (4.20)$$

### 4.3 SPECTRAL SIGNATURES

In Chapter 2 we have seen how the interaction between light and matter can lead to absorption peaks at certain frequencies that are resonant with the transition between different energy levels in a system. The equilibrium occupation of these energy levels is given by the Boltzmann distribution. At room temperature ( $k_B T \approx 200 \text{ cm}^{-1}$ ), this means that for modes with vibrational transition frequencies  $> 1400 \text{ cm}^{-1}$  practically only the ground-state energy level is occupied ( $> 99.9\%$ ). The linear absorption spectra of vibrational modes in this frequency region thus mostly reflects their  $\nu = 0 \rightarrow 1$  transitions.

On the other hand, in our pump-probe experiments we observe the pump induced absorption *changes* in a sample. This means that the spectral signatures we observe are not the absorption peaks themselves, but the effect of the

pump on these absorption peaks. The observed vibrational transient spectra fall into two categories. First there the direct effects resulting from the absorption changes associated with excitation of the mode itself. As we have seen in Section 2.5.4 the excitation of an anharmonic oscillator leads to a bleach at frequencies around the original ( $\nu = 0 \rightarrow 1$ ) linear absorption and an induced absorption at lower frequencies ( $\nu = 1 \rightarrow 2$ ). Secondly, there are the indirect effects of changes to the environment that may affect the frequency and absorption cross-section of the mode.

For example, after an excitation decays, the energy is released and goes into other modes that can be in proximity to the original excitation. If these other modes are (anharmonically) coupled to the original mode they can be observed in the transient spectra as a shift of the original (linear absorption) frequency or a change in the total absorption cross-section. For example, the thermalization of the O–H stretch mode in water leads to the occupation of low frequency modes that manifests as a decreased and blue-shifted absorption spectrum (see Fig. 4.4). Another example is the shift in frequency of the carbonyl stretch mode of acetate upon the arrival of a proton (see Chapter 8)

Absorption peaks generally consist of an inhomogeneously broadened collection of homogenous absorption line shapes (i. e. Lorentzian see Section 2.3.3). Depending on the mechanism behind the inhomogeneous broadening, the cross-section of the underlying peaks may vary. For example, the inhomogeneous broadening of the O–H stretch mode in liquid water is primarily caused by (Gaussian) fluctuations in the associated hydrogen bond strength. The transition frequencies are non-linearly dependent on the hydrogen bond fluctuations leading to an asymmetric distribution of the absorption peaks, more stretched towards the red side (see Fig. 1.5). In general, a linear absorption peak is well described using the convolution of an asymmetric distribution with a Lorentzian line shape. The absorption difference spectra can generally be described as the sum of a negative peak at the frequency of the original absorption and a positive peak at the new position of the absorption. A change in the total cross-section can be accounted for by different amplitudes of the two peaks.

In most cases, described in this thesis, we are primarily interested in a model that describes the evolution of states in the time-domain. In such cases we fit the temporal dynamics while simply calculating (not fitting) the associated spectra using spectral decomposition. A notable exception is the case of spectral diffusion in Chapter 7, where we excite a non-equilibrium sub-ensemble within an inhomogeneously broadened absorption band. The minimum width of such a sub-ensemble is determined by the homogeneous line width of the underlying spectra. Fluctuations that underly the inhomogeneous broadening lead to redistribution of the frequencies in the excited sub-ensemble until the equilibrium distribution is obtained. During the course of spectral diffusion, the spectral signatures of a mode are no longer constant, which means that we can not use the spectral decomposition methods to model the data and instead have to fit both the spectra and the time dynamics.

## 4.4 UNIMOLECULAR REACTIONS

### 4.4.1 RATE MATRIX

The time dynamics in a data set depend on the reaction<sup>a</sup> pathways of the constituent populations. In a first-order (unimolecular) reaction, the rates depend linearly on the concentrations of the reactants:

$$\frac{dN_i(t)}{dt} = \sum_j -k_{i \rightarrow j} N_i(t) + k_{j \rightarrow i} N_j(t), \quad (4.21)$$

where  $k_{i \rightarrow j}(t)$  are the rate constants for the reaction  $N_i \rightarrow N_j$  and vice versa for  $k_{j \rightarrow i}(t)$ . Negative terms in the rate equations lead to decay of the population and positive terms lead to ingrowth. In this case the rate constants  $k$  are all time-independent and it is convenient to write the rate equations (4.21) in the form of a matrix as:

$$\frac{d}{dt} N_i(t) = \sum_j K_{ij} N_j(t), \quad (4.22)$$

where the rate matrix  $K_{ij}$  contains all the transition rates  $k_{i \rightarrow j}$  and  $k_{j \rightarrow i}$ . It can be shown that if the sum of each column of the rate matrix equals zero, we are dealing with a closed system, i. e. no population enters or leaves the system and the total population remains constant.

Eq. (4.22), constitutes a set of linear ordinary differential equations (ODE). These linear ODEs can be solved in general by diagonalizing the rate matrix  $K$  as follows. First we construct from the *eigenvalues* of  $K$  a diagonal matrix  $D$  and from the *eigenvectors* of  $K$  a matrix  $V$ , such that the following equation holds:

$$K V = V D \quad (4.23)$$

We use matrix  $V$  to construct a new vector  $\vec{M}(t)$  such that

$$\vec{N}(t) = V \vec{M}(t) \quad (4.24)$$

We can now diagonalize the original problem:

$$\frac{d}{dt} \vec{N}(t) = \frac{d}{dt} (V \vec{M}(t)) = K (V \vec{M}(t)) = V D \vec{M}(t) \quad (4.25)$$

$$\Rightarrow \frac{d}{dt} \vec{M}(t) = D \vec{M}(t) \quad (4.26)$$

The set of equations,  $\vec{M}(t)$ , can be solved straightforwardly because  $D$  is diagonal:

$$\vec{M}(t) = \exp(Dt) \vec{M}(0) = \exp(Dt) V^{-1} N(0) \quad (4.27)$$

Finally we can transform the obtained solution for  $\vec{M}(t)$  back to  $\vec{N}(t)$  with Eq. (4.24):

$$\vec{N}(t) = V \exp(Dt) V^{-1} \vec{N}(0) \quad (4.28)$$

---

<sup>a</sup>In the current context 'reaction' may refer to any change in state of the system.

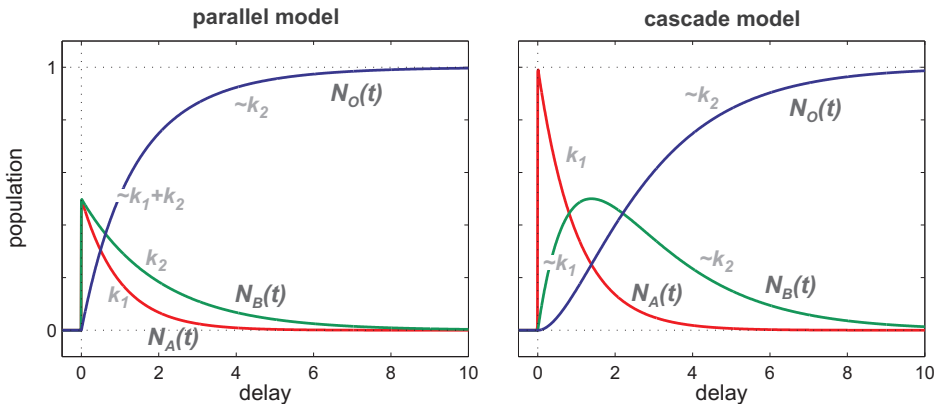


FIGURE 4.5. Typical population dynamics of three-state parallel and cascade models.

From these equations we can conclude that the time-dependent population of a unimolecular reaction scheme is always described as a linear combination of exponentials where the rates are the eigenvalues of the rate matrix. As a consequence, it can be shown that if no information is available on the spectral signatures of a multi-component data set, any model whose rate equation matrix has the same eigenvalues will fit equally well to this data set. In such cases the quality of the fit ( $\chi^2$ ) can not be used to determine which model is best and the distinction between models relies on the physical meaning of the least-squares associated spectra and/or anisotropy.

We will next discuss two basic examples of models that are commonly encountered when analyzing the time-dependent dynamics of a data set: the 'parallel model' and the 'cascade model'.

#### 4.4.2 PARALLEL MODEL

First, we consider a reaction scheme where a set of populations in state  $A, B, \dots$  transfer independently (parallel) with respective rates  $k_1, k_2, \dots$  to a common end state  $O$ :



For this example, we limit the number of parallel channels to two. Together with the end state this gives us three states. The time-dependent population dynamics  $N_i$  of this three-state parallel model are described by

$$\frac{d}{dt} \begin{pmatrix} N_A(t) \\ N_B(t) \\ N_O(t) \end{pmatrix} = \begin{bmatrix} -k_1 & 0 & 0 \\ 0 & -k_2 & 0 \\ +k_1 & +k_2 & 0 \end{bmatrix} \begin{pmatrix} N_A(t) \\ N_B(t) \\ N_O(t) \end{pmatrix}. \quad (4.31)$$

Although the solutions to these rate equations are straightforward we proceed to use the methods of Section 4.4.1 as an illustrative example. Using linear algebra, we extract from the rate matrix  $K$  in Eq. (4.31) the eigenvalue matrix  $D$  and corresponding eigenvector matrix  $V$ :

$$D = \begin{bmatrix} -k_1 & 0 & 0 \\ 0 & -k_2 & 0 \\ 0 & 0 & 0 \end{bmatrix}, \quad V = \begin{bmatrix} -1 & 0 & 0 \\ 0 & -1 & 0 \\ 1 & 1 & 1 \end{bmatrix}. \quad (4.32)$$

Coincidentally, in this particular case  $V^{-1} = V$ . We thus fill in the values for  $D$  and  $V$  into Eq. (4.28)

$$\begin{pmatrix} N_A(t) \\ N_B(t) \\ N_O(t) \end{pmatrix} = \begin{bmatrix} -1 & 0 & 0 \\ 0 & -1 & 0 \\ 1 & 1 & 1 \end{bmatrix} \begin{bmatrix} e^{-k_1 t} & 0 & 0 \\ 0 & e^{-k_2 t} & 0 \\ 0 & 0 & 1 \end{bmatrix} \begin{bmatrix} -1 & 0 & 0 \\ 0 & -1 & 0 \\ 1 & 1 & 1 \end{bmatrix} \begin{pmatrix} N_A(0) \\ N_B(0) \\ N_O(0) \end{pmatrix} \quad (4.33)$$

yielding solutions:

$$\begin{aligned} N_A(t) &= N_A(0) e^{-k_1 t} \\ N_B(t) &= N_B(0) e^{-k_2 t} \\ N_O(t) &= 1 - N_A(0) e^{-k_1 t} - N_B(0) e^{-k_2 t} \end{aligned} \quad (4.34)$$

This reaction scheme is commonly encountered when multiple independent components are present in a data set, e. g. the overlapping spectral responses of bulk and anion-bound water molecules in Chapter 10.

### 4.4.3 CASCADE MODEL

Next, let us consider a slightly more complicated reaction scheme where the population starts in state  $A$  and is transferred consecutively with rates  $k_1, k_2, \dots$  through a number of states  $B, C, \dots$ :



In the reactions, the population is usually cascading down an energy level diagram. In principle this reaction scheme could be extended to include an arbitrary amount of states, but for most cases three suffice. The time-dependent population dynamics  $N_i$  of this three-state cascade model are described by

$$\frac{d}{dt} \begin{pmatrix} N_A(t) \\ N_B(t) \\ N_C(t) \end{pmatrix} = \begin{bmatrix} -k_1 & 0 & 0 \\ +k_1 & -k_2 & 0 \\ 0 & +k_2 & 0 \end{bmatrix} \begin{pmatrix} N_A(t) \\ N_B(t) \\ N_C(t) \end{pmatrix}. \quad (4.36)$$

Using again the methods described in Section 4.4.1 we find solutions:

$$\begin{aligned} N_A(t) &= N_A(0) e^{-k_1 t} \\ N_B(t) &= N_A(0) \frac{k_1}{k_2 - k_1} (e^{-k_1 t} - e^{-k_2 t}) \\ N_C(t) &= N_A(0) \left( 1 + \frac{k_1 e^{-k_2 t} - k_2 e^{-k_1 t}}{k_2 - k_1} \right). \end{aligned} \quad (4.37)$$

This three-state consecutive model is used for example to describe the vibrational energy relaxation of the O–H stretch mode in water, see Chapter 5. Note that the solutions in Eqs. (4.34) and (4.37) both consist of a linear combination of exponentials with rate constants  $k_1$  and  $k_2$ . These two models can thus only be distinguished on the basis of their associated spectra.

## 4.5 PSEUDO-UNIMOLECULAR REACTIONS

### 4.5.1 SURVIVAL PROBABILITY

Until now we have considered unimolecular reactions  $A \rightarrow B$  that depend only on the presence (concentration) of the reactant  $A$  itself. However there also exist reactions that depend on the proximity of two or more reactant. In the case of a bimolecular reaction,  $A + B \rightarrow C$ , two reactants  $A$  and  $B$  are combined and lead to a new product state  $C$ . A typical example of such a reaction are the proton transfer reactions described in Chapters 8 and 9, where the reaction rate is dependent on the proximity of acid and base molecules. Also the rate of Förster transfer, described in Chapters 10 and 11, is dependent on the proximity of two reactants, in this case the donor and acceptor vibrational modes.

The description of these reactions is simplified substantially if we work in the pseudo-unimolecular limit, where one of the reactants is in large excess and the reaction is irreversible. We describe the reaction



where  $A$  reacts competitively to any  $B_i$  with unimolecular rate  $k_i$ , resulting in reaction product  $C_i$ . To solve this reaction scheme, we define the 'probability density' of the unreacted complexes:

$$\varphi_i(t) = \langle A + B_i \rangle(t). \quad (4.39)$$

If we assume that  $A$  is dilute enough that we may describe each reaction complex independently,  $\varphi_i(t)$  decays with the unimolecular rate  $k_i$  independent of the concentration of  $A$ . The reaction rate of  $A$  depends both on  $k_i$  and  $\varphi_i$ . These

assertions leads us to the following set of rate equations:

$$\frac{d\varphi_i(t)}{dt} = -k_i \varphi_i(t), \quad (4.40)$$

$$\frac{dA(t)}{dt} = -\sum_i k_i \varphi_i(t) A(t), \quad (4.41)$$

$$\frac{dC_i(t)}{dt} = +k_i \varphi_i(t) A(t). \quad (4.42)$$

The solution to Eq. (4.40) is straightforward and can be written as

$$\varphi_i(t) = \lambda_i \exp(-k_i t), \quad (4.43)$$

where we have defined  $\lambda_i = \varphi_i(0)$ , i. e. the average the number of  $B$  with which  $A$  can react through channel  $i$ .

The solutions to Eqs. (4.41) and (4.42) can be written implicitly as:

$$A(t) = A(0) \exp\left(-\int_0^t dt' \sum_i k_i \varphi_i(t')\right), \quad (4.44)$$

$$C_i(t) = C_i(0) + \int_0^t dt' k_i \varphi_i(t') A(t'). \quad (4.45)$$

The term  $\sum_i k_i \varphi_i(t)$  in Eq. (4.44) is dubbed the 'reactive flux' and is equivalent to a time-dependent reaction rate  $k_{A+B \rightarrow C}(t)$ . We note that Eq. (4.45) can be used to keep track of the number of reactions through channel  $i$ . By explicitly performing the integration of Eq. (4.44) by filling in Eq. (4.43) we find:

$$A(t) = A(0) \exp\left[-\sum_i \lambda_i (1 - e^{-k_i t})\right] \quad (4.46)$$

The validity of Eq. (4.46) can be easily checked by differentiation. To better grasp its implications, we examine the 'survival probability'  $S(t) = A(t)/A(0)$ :

$$S(t) = \exp\left[-\sum_i \lambda_i (1 - e^{-k_i t})\right] \quad (4.47)$$

$$= \prod_i \exp[-\lambda_i (1 - e^{-k_i t})] \quad (4.48)$$

$$= \prod_i e^{-\lambda_i} \exp[\lambda_i e^{-k_i t}] \quad (4.49)$$

$$= \prod_i e^{-\lambda_i} \sum_{n_i=0}^{\infty} \frac{(\lambda_i e^{-k_i t})^{n_i}}{n_i!} \quad (4.50)$$

$$= \prod_i \sum_{n_i=0}^{\infty} \frac{e^{-\lambda_i} \lambda_i^{n_i}}{n_i!} e^{-n_i k_i t}, \quad (4.51)$$

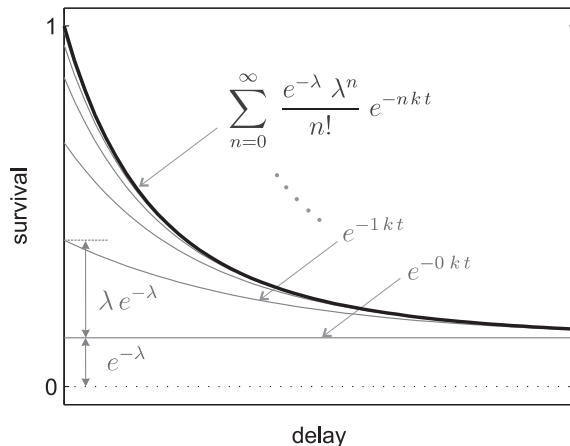


FIGURE 4.6. Decomposed survival probability as in Eq. (4.51). Thin lines show the individual rates with  $n$  reactants. Thick line shows the total sum which equals Eq. (4.47) for one component  $i$ .

where we used in step Eq. (4.50) the Taylor expansion for the exponential function. Eq. (4.51) shows that the survival probability  $S$  is the product of the individual survivals  $S_i$ :

$$S(t) = \prod_i S_i(t) \quad (4.52)$$

with

$$S_i(t) = \sum_{n_i=0}^{\infty} P_{n_i}(\lambda_i) e^{-n_i k_i t}, \quad (4.53)$$

where  $P_n(\lambda)$  is the probability in Poisson statistics to find  $n$  occurrences for an event which has an average chance  $\lambda$ . We thus recognize the individual survival probability  $S_i$  equals a sum over all possible configurations  $n_i = 0 \cdots \infty$ , each weighted by the Poisson statistical chance of occurrence (see also Fig. 4.6). The survival probability for that particular configuration equals  $\exp(n_i k_i t)$ , i. e. the unimolecular rate is multiplied by the number of reaction pathways. Note that if  $\lambda$  is small enough, there is a substantial chance  $P_0(\lambda) = e^{-\lambda}$  that no reaction will take place ( $n_i = 0$ ). In terms of the reactants  $A$  and  $B$  this means that only if  $B(0) \gg A(0)$  all  $A$  will react.

#### 4.5.2 CONCENTRATION DEPENDENCE

To see how the survival probability of reactant  $A$  depends on the concentration of  $B$ , we define

$$\lambda_i = \rho V_i \quad (4.54)$$

where  $\rho$  is the concentration of  $B$  (units  $1/L^3$ , where  $L$  is a length scale) and  $V_i$  is the 'reactive volume' (units  $L^3$ ). Filling Eq. (4.54) into Eq. (4.47) we find

$$S(t) = \exp \left[ -\rho \sum_i V_i (1 - e^{-k_i t}) \right]. \quad (4.55)$$

For  $t \rightarrow \infty$  we see that Eq. (4.55) tends to  $\exp[-\rho \sum_i V_i]$ . The end level of the survival thus reflects the total reactive volume

$$\sum_i V_i = \frac{-\ln[S(\infty)]}{\rho}. \quad (4.56)$$

Eq. (4.55) is a specific case for the survival probability of the generalized Smoluchowski form [153]:

$$S(t) = \exp[-\rho P(t)]. \quad (4.57)$$

where  $P(t)$  is the pair reaction probability. This equation holds true for any pseudo-unimolecular reaction. Vice versa, we can check if a data set can be described with pseudo-unimolecular kinetics by varying the concentration. Let us consider two data sets with concentrations of reactant  $B = \rho_1$  and  $B = \rho_2$  for which we measure survival probabilities  $S_1(t)$  and  $S_2(t)$ , respectively. Then according to Eq. (4.57) we should find:

$$S_1(t) = \exp \left( -\frac{\rho_1}{\rho_2} \ln[S_2(t)] \right), \quad (4.58)$$

i. e. independent of the functional form of  $P(t)$ . This procedure, dubbed 'concentration scaling', is used to check the applicability of Eq. (4.57) in Chapter 9 (see e. g. Fig. 9.6). Its validity is only guaranteed if the conditions for pseudo-unimolecular reactions are fulfilled, i. e. one of the reactants is in large excess and the reaction is irreversible.

### 4.5.3 CONTINUUM LIMIT

We now extend Eqs. (4.40)–(4.42) to the continuum limit. As before, we set  $k_{ij} = 0$ , i. e. we neglect diffusion. We consider a spherically symmetric system with  $A$  at the center and a uniform concentration  $\rho$  of reactants  $B$  for distances  $r > r_{\min}$  (excluded volume). The reaction rate  $k(r)$  depends only on the distance  $r$  between  $A$  and  $B$ . In the continuum limit we substitute:

$$\begin{aligned} k_i &\rightarrow k(r), \\ \varphi_i(t) &\rightarrow \varphi(r, t), \\ \lambda_i &\rightarrow \rho 4\pi r^2 dr, \end{aligned}$$

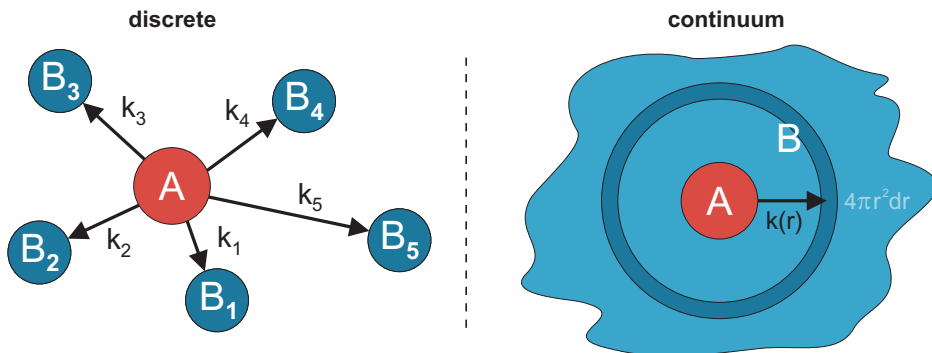


FIGURE 4.7. Discrete versus continuum: pseudo-unimolecular reaction of  $A$  with excess  $B$ . Survival of individual reactant  $A$  depends on the combined chance to react with any  $B$ . Left: Different reactive volumes  $B_i$  have different unimolecular reaction rates  $k_i$ . Right: unimolecular rate  $k$  is a continuous function of distance  $r$  for a shell with reactive volume  $4\pi r^2 dr$ .

and replace the summation with an integral over  $r$ :

$$\frac{\partial \varphi(r, t)}{\partial t} = -k(r) \varphi(r, t), \quad (4.59)$$

$$\frac{dA(t)}{dt} = -\int_r \varphi(r, t) A(t), \quad (4.60)$$

$$\frac{\partial C(r, t)}{\partial t} = +k(r) \varphi(r, t) A(t), \quad (4.61)$$

with solutions

$$\varphi(r, t) = \rho 4\pi r^2 dr \exp(-k(r) t), \quad (4.62)$$

$$A(t) = A(0) \exp\left(\rho \int_0^t dt' \int_{r_{\min}}^{\infty} dr 4\pi r^2 k(r) \varphi(r, t')\right), \quad (4.63)$$

$$C(r, t) = C(r, 0) + \int_0^t dt' k(r) \varphi(r, t') A(t'), \quad (4.64)$$

where  $C(r, t)$  is the distance distribution of reactions  $A + B \rightarrow C$  up to time  $t$ .

Analogous to Eq. (4.47), the survival probability of  $A$  can be calculated explicitly by integrating Eq. (4.63) over  $t$ :

$$S(t) = \exp\left(-\rho \int_{r_{\min}}^{\infty} dr 4\pi r^2 (1 - e^{-k(r)t})\right). \quad (4.65)$$

This equation can be used to describe any type of distance dependent pseudo-unimolecular reaction  $k(r)$ . It is used in Chapters 8 and 10 where diffusion is neglected, with different functional forms for  $k(r)$ .

The distance distribution of transfer events  $C(r, t)$  in Eq. (4.64) can be worked out further as

$$C(r, t) = \rho 4\pi r^2 dr k(r) A(0) \int_0^t dt' e^{-k(r)t'} S(t'), \quad (4.66)$$

where we set  $C(r, 0) = 0$  and  $S(t)$  is given by Eq. (4.65). To get the total distance distribution  $C(r)$  we evaluate Eq. (4.67) at  $t = \infty$ :

$$C(r) = \rho 4\pi r^2 dr k(r) A(0) \int_0^\infty dt e^{-k(r)t} S(t). \quad (4.67)$$

#### 4.5.4 DIFFUSION

For a distance dependent reaction rate  $k(r)$ , pairs that are in close proximity to each other generally react faster than those further away. As these close reaction pairs get depleted, a non-uniform distribution of pair reaction distances is created. In general, diffusion will act to counteract this non-uniformity by the exchange of pair reaction distances. In the continuum limit, this process can be described by diffusion equations which can take various forms depending on the geometry and dimensionality of the system.

In the present case we consider a spherically symmetric system and replace Eq. (4.59) by adding a diffusion term:

$$\frac{\partial \varphi(r, t)}{\partial t} = -k(r) \varphi(r, t) + \frac{D}{r^2} \frac{\partial}{\partial r} r^2 \frac{\partial}{\partial r} \varphi(r, t). \quad (4.68)$$

The first part on the right hand side of Eq. (4.68) represents the distance dependent sink term and the second part represents the diffusion of the probability density, where  $D$  is the diffusion coefficient between reactants  $A$  and  $B$ . The relative importance of diffusion obviously depends on the coefficient  $D$  in relation to  $k(r)$ . In the limiting case where diffusion is negligible we can simply revert to the previously derived Eq. (4.65). In the other limit, e.g. where the only reactions that can take place are at 'contact distance',  $k(r)$  is reduced to a delta function and the reaction is fully dictated by the diffusion rate.

In any case, it can be shown that also for diffusion influenced reactions, the survival probability of  $A$  still adheres to the Smoluchowski survival of Eq. (4.57). There are some analytical approximations to  $S(t)$  for specific forms of  $k(r)$  [36, 169], but not for a more general distance-dependence. In Chapter 8 we therefore use numerical integration to solve the diffusion and rate equations.

## 4.6 FÖRSTER TRANSFER

**DIPOLE-DIPOLE COUPLING** Förster energy transfer results from a near-field (non-radiative) dipole-dipole coupling between an excited-state donor molecule whose emission spectrum overlaps with that of a nearby acceptor molecule. In

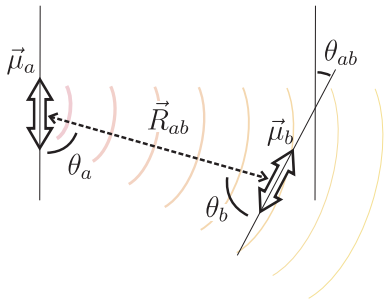


FIGURE 4.8. Spatial geometry of a dipole-dipole interaction.

general, the rate of Förster energy transfer  $k_F$  between two dipole oscillators  $a$  and  $b$  is proportional to the expression [47, 102, 165]:

$$k_{F,ab} \propto \frac{|\vec{\mu}_a|^2 |\vec{\mu}_b|^2 \kappa_{ab}^2}{|\vec{R}_{ab}|^6} \int d\nu \sigma_a(\nu) \sigma_b(\nu), \quad (4.69)$$

where  $\vec{\mu}_a$  and  $\vec{\mu}_b$  are the transition dipole moments of the transmitting and receiving dipole modes,  $\vec{R}_{ab}$  is the distance vector between the dipoles,  $\sigma_a$  and  $\sigma_b$  are the normalized vibrational line shapes of the two modes, and  $\kappa_{ab}$  is a geometrical factor expressing the relative orientations of the dipole moments (see Fig. 4.8):

$$\kappa_{ab} = \hat{\mu}_a \cdot \hat{\mu}_b - 3(\hat{\mu}_a \cdot \hat{R}_{ab})(\hat{\mu}_b \cdot \hat{R}_{ab}) \approx \cos \theta_{ab} + 3 \cos \theta_a \cos \theta_b, \quad (4.70)$$

where the hats denote normalized unit vectors. The latter equality only holds if all vectors  $\hat{\mu}_a$ ,  $\hat{\mu}_b$ , and  $\hat{R}_{ab}$  lie in a plane as drawn in Fig. 4.8.

**FÖRSTER RADIUS** If we assume that the relative orientation of dipole oscillators  $a$  and  $b$  is unrelated to their distance  $r$ , we can write the rate of Förster transfer  $k_F$  phenomenologically as:

$$k_F(r) = \frac{\hat{k}_F}{r^6} \equiv \frac{1}{T_1} \left( \frac{R_0}{r} \right)^6, \quad (4.71)$$

where  $\hat{k}_F$  is the rate of Förster transfer at  $R = 1$ ,  $T_1$  is the default donor lifetime in the absence of Förster transfer, and  $R_0$  is the Förster radius. This Förster radius is defined as the distance where  $k_F = 1/T_1$ , meaning that half the vibrational energy is dissipated through Förster transfer.

**SURVIVAL** There are many systems, in which the Förster transfer process can be described by pseudo-unimolecular reaction dynamics. Examples include the loss of vibrational energy as a result of Förster energy transfer in Chapter 10 and the decay of anisotropy in Chapter 11. In the continuum description of such systems, we can use Eq. (4.65) to describe the survival probability of the

original direction or excitation. Filling in the distance dependence of Eq. (4.71) into Eq. (4.65), we get:

$$S(t) = \exp \left\{ -\rho \int_{r_{\min}}^{\infty} dr 4\pi r^2 \left( 1 - \exp \left[ -\frac{1}{T_1} \left( \frac{R_0}{r} \right)^6 t \right] \right) \right\}. \quad (4.72)$$

where  $\rho$  is the concentration of Förster receivers. If we take a minimum transfer radius  $r_{\min} = 0$  and explicitly perform the integration over all distances we find

$$S(t) = \exp \left( -\rho \frac{4}{3} \pi \frac{3}{2} \sqrt{\frac{R_0^6 t}{T_1}} \right) \quad (4.73)$$

which is equivalent to the formula developed by Förster [47]. Note that the survival dynamics are highly non-exponential as they depend on  $\sqrt{t}$ .